Available online at www.sciencedirect.com
ScienceDirect
Trans. Nonferrous Met. Soc. China 35(2025) 1679−1690
Transactions of Nonferrous Metals Society of China
www.tnmsc.cn

Effect of slag basicity on semi-molten smelting process of saprolitic and limonitic laterite ores

Yu-xiao XUE[1,2], Jian-bo ZHAO[1,2], Zhi-xiong YOU[1,2], Xue-wei LV[1,2]

1. College of Materials Science and Engineering, Chongqing University, Chongqing 400044, China;
2. Chongqing Key Laboratory of Vanadium−Titanium Metallurgy and New Materials, Chongqing University, Chongqing 400044, China

Received 19 November 2023; accepted 6 August 2024

Abstract: The semi-molten smelting process of a mixture of saprolitic and limonitic laterite ores was systematically investigated and the effect of slag basicity was deeply analyzed. The results indicate that the slag system can be located in the liquidus region of low melting-point diopside ($CaMgSi_2O_6$) when slag basicity is kept at 0.3 and limonitic laterite mass fraction is not less than 10%. When the reduction temperature, C/O mass ratio, limonitic laterite mass fraction and slag basicity are kept at the optimum values of 1300 °C, 0.86, 20% and 0.3, respectively, ferronickel products with grades 6.42% Ni and 86.99% Fe are prepared. The recovery rates of Ni and Fe reach 88.60% and 72.25%, respectively.
Key words: ferronickel; saprolitic laterite ore; limonitic laterite ore; slag basicity; semi-molten smelting process

1 Introduction

With the increasing depletion of nickel sulfide resources, nickel laterite resources have been converted into the primary source of nickel for stainless steel production [1,2]. Presently, pyrometallurgical processes for ferronickel production encompass the sintering−blast furnace (BF) process, rotary kiln−electric furnace (RKEF) process and direct reduction−magnetic separation (DRM) process [3−5]. The DRM process stands out for its lower smelting temperature, less energy consumption and simpler process flow compared with the former two methods [6,7]. In addition, saprolitic laterite ore possesses higher nickel grade and lower iron grade than limonitic laterite ore. The former laterite ore is more suitable for the DRM process due to the selective reduction properties of nickel [8].

The DRM process includes two types, i.e., solid-state reduction and semi-molten smelting processes [9−11]. In the latter process, the aggregation and growth of ferronickel grains are easier to be achieved due to the higher reduction temperature. The temperature generally reaches 1200−1400 °C. Currently, numerous studies are concentrated on the strengthening of the semi-molten smelting process of nickel laterite. The optimization of slag compositions is the major method [12−15]. Saprolitic laterite inherently contains high contents of SiO_2 and MgO. An increase in SiO_2 content promotes the formation of fayalite. However, it is adverse to the recovery of metallic elements due to its poor reducibility [16]. In addition, the aggregation and growth of ferronickel grains would be hindered at an excessive content of MgO due to the formation of magnesium silicate [17]. Although a rise in Al_2O_3 content is beneficial to the destruction of the

Corresponding author: Zhi-xiong YOU, Tel: +86-18306089886, E-mail: youzx@cqu.edu.cn
https://doi.org/10.1016/S1003-6326(25)66775-6

magnesium silicate structure, the formation of alloy phase would be suppressed due to the substitution of Al^{3+} ions for Fe^{3+} ions in magnetite lattice [18]. An appropriate increase of FeO content of slag is not only instrumental in the processing of carburization reaction, but also favorable to the reduction of the melting point and viscosity of slag. The better conditions can be provided for the aggregation and growth of ferronickel grains [19]. Similarly, the slag basicity (i.e., the mass ratio of CaO/SiO_2) should also be appropriate. When slag basicity is too high, the refractory phases such as akermanite would be massively formed. It is adverse to the slag−alloy separation [20].

The co-utilization of saprolitic and limonitic laterite ores was proposed for the more effective smelting of ferronickel. SUHARNO et al [21] mainly investigated the reduction kinetics of the two nickel laterite ores. However, the reduction temperature was maintained at 950−1150 °C, which was suitable for the solid-state reduction process rather than the semi-molten smelting process. In our prior study [22], ferronickel with 8.08 wt.% Ni, 80.09 wt.% Fe and 3.75 wt.% C was obtained via the semi-molten smelting process when the reduction temperature, carbon mass fraction and limonitic laterite mass fraction were 1380 °C, 6% and 5%, respectively. However, the reduction temperature was higher and slag basicity was not optimized. Although TIAN et al [23] conducted a research on the reduction process of a mixture of saprolitic and limonitic laterite ores, the nickel content in the magnetic fraction was not high enough. In addition, the serious ring-forming problem was inevitable in the rotary kiln [24]. The relevant problems can be nicely avoided in the rotary hearth furnace [22]. However, the effect of slag basicity on the semi-molten smelting process of the blended laterite ores in the rotary hearth furnace is still unclear nowadays.

The semi-molten smelting process of saprolitic and limonitic laterite ores based on the rotary hearth furnace method was investigated in this study. The thermodynamics and melting characteristics of slag were systematically studied. The parameters of semi-molten smelting process including reduction temperature, C/O mass ratio, limonitic laterite mass fraction and slag basicity were optimized. The growth characteristics of ferronickel grains were analyzed.

2 Experimental

2.1 Raw materials

The adopted raw materials mainly included two types of laterite ores, a reductant of bituminous coal and a series of analytical reagents. The laterite ores were both imported from the Philippines. The bituminous coal was provided by a steel plant in China. The analytical reagents were purchased from Aladdin Company. As shown in Table 1, saprolitic laterite possesses higher contents of TNi, MgO and SiO_2 compared with limonitic laterite. However, the contents of TFe, Cr_2O_3 and Al_2O_3 in the former laterite ore are lower. In addition, the levels of LOI in the two laterite ores are similar. As illustrated in Fig. 1, saprolitic laterite mainly contains $(Mg,Fe,Ni)_3Si_2O_5(OH)_4$ and a small amount of FeO(OH) and SiO_2. Limonitic laterite is composed of FeO(OH) and a slight amount of $(Mg,Fe,Ni)_3Si_2O_5(OH)_4$, $Fe_2O_3{\cdot}nH_2O$ and SiO_2. Bituminous coal contains a fixed carbon content of 74.22%, which is used as the reductant for the semi-molten smelting process (Table 2). The analytical reagents of SiO_2, MgO, CaO, Al_2O_3 and FeO are used for the simulation of slag compositions. The size distributions of raw materials are all kept below 0.074 mm.

2.2 Experimental procedure

2.2.1 Characterization methods

The chemical compositions of samples were determined by means of inductively coupled plasma atomic emitted spectrometer (ICP-AES, optima 8000, PerkinElmer, Singapore). The LOI of nickel laterite ores was measured at 1100 °C for 3 h in air atmosphere. The mineral occurrence states of samples were determined by the analysis of X-ray

Table 1 Chemical compositions of nickel laterite ores (wt.%)

Ore	TNi	TFe	Cr_2O_3	MgO	SiO_2	Al_2O_3	CaO	LOI
Saprolitic laterite	1.73	21.09	1.53	20.88	28.49	0.86	0.24	13.82
Limonitic laterite	0.83	44.41	4.34	3.74	7.12	3.97	0.62	14.26

TNi: Total Ni content; TFe: Total Fe content; LOI: Loss on ignition

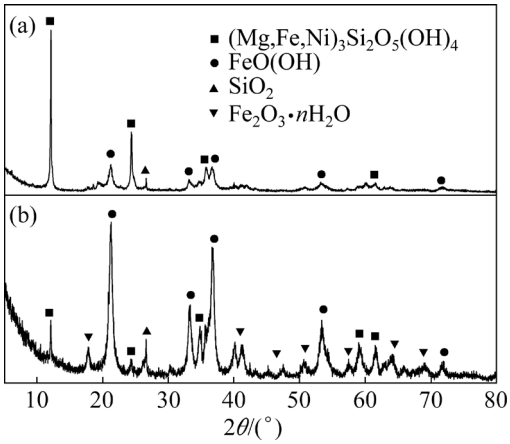

Fig. 1 XRD patterns of nickel laterite ores: (a) Saprolitic laterite; (b) Limonitic laterite

Table 2 Proximate analysis results of bituminous coal (wt.%)

Fixed carbon (FC_{daf})	Ash (A_d)	Volatile (V_{daf})
74.22	21.56	9.6

d: Dry basis; daf: Dry ash free basis

diffraction (XRD, D/max−2500 X, Rigaku, Japan). The tests were operated at 40 kV in step mode within a range of 2θ from 0° to 80°. The step width of 2θ was 0.02° and the count time of per step was 0.5 s. The proximate analysis of bituminous coal was conducted in the light of the standard of GB/T 212—2008. Thermodynamic analysis was conducted by means of the sectors of Phase Diagram and Equilib in FactSage-8.0 software. The mineralogy of samples was investigated by means of the optical microscope (Leica DM4P, Leica Camera AG, Germany). The colors of pores and mineral phases presented in the optical micrographs were different. The software of Image-Pro Plus 6.0 was used for the determination of the number and total area of ferronickel grains. The average diameter of ferronickel grains was calculated as follows:

$$d = 2\sqrt{\frac{S}{n\pi}} \tag{1}$$

where d is the average diameter of ferronickel grains, μm; S is the total area of ferronickel grains in the optical micrographs, μm^2; n is the number of ferronickel grains in the optical micrographs.

2.2.2 Determination of slag melting characteristics

As shown in Fig. 2, the melting characteristics of slag were determined in a high-temperature horizontal tube furnace equipped with a high-resolution digital camera. Analytical reagents including SiO_2, MgO, CaO, Al_2O_3, and FeO were uniformly blended and then compacted into a cylinder with a diameter of 3 mm and a height of 5 mm. Subsequently, the cylinder of slag was placed on a square corundum substrate with a length of 5 mm and a thickness of 3 mm. After the substrate was loaded into the horizontal tube furnace, the heating program was started with a heating rate of 5 °C/min. The slag was gradually melted in an argon atmosphere. The melting process was recorded by the high-resolution digital camera and the photos were captured at a rate of 1 frame/s. When the slag height in the photos was reduced to 1/4, 2/4 and 3/4 of its initial value, the corresponding temperature was the softening temperature, hemisphere temperature and flow temperature, respectively.

2.2.3 Direct reduction−magnetic separation tests

In the direct reduction−magnetic separation tests, the reduction temperature, C/O mass ratio, limonitic laterite mass fraction and slag basicity varied from 1250 °C, 0.80, 10% and 0.1 to 1325 °C, 1.10, 40% and 0.5, respectively. The detailed experimental procedure was shown as follows.

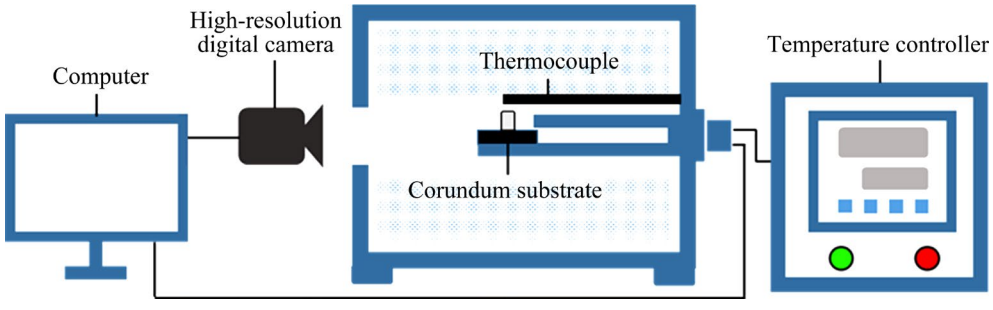

Fig. 2 Schematic diagram of melting characteristic measurement equipment

The direct reduction tests were conducted in a vertical resistance furnace (GSL−1700X-VT, Kejing Group, China). The dried raw materials including saprolitic laterite, limonitic laterite, bituminous coal and CaO reagent were uniformly blended and then compacted into cylindrical briquettes with a diameter of 15 mm and a height of 10 mm. The applied pressure was kept at 10 MPa. As shown in Fig. 3, the briquettes were placed in a graphite crucible with a diameter of 70 mm and a height of 120 mm. When the temperature of the vertical resistance furnace reached 800 °C, the graphite crucible was introduced and then heated to the target temperature in an argon atmosphere at a heating rate of 10 °C/min. After that, the reduced samples were immediately removed from the furnace and quenched in water. Eventually, the reduced samples were dried in a vacuum oven.

The reduced samples were preliminarily crushed by means of a jaw crusher with an opening size of 1 mm. Then, the wet ball-milling tests were conducted in a ball mill (XMQ-*d*150 mm × 50 mm, Yetuo Technology Co., Ltd., China). The duration of the ball-milling process was set at 10 min. The obtained ore pulp was introduced into a magnetic tube (XCGS−50, Exploration Machinery Co., Ltd., China) for the separation of magnetic and non-magnetic fractions. The magnetic induction current was kept at 1 A. The two fractions were dried in a vacuum oven and then weighed. The recovery rates of Ni and Fe were calculated as follows. The growth characteristics of ferronickel grains were assessed based on the mineralogy of the reduced briquettes. The relevant methods were presented in Section 2.2.1.

$$\beta_{\mathrm{Ni}}=\frac{m_4\cdot\alpha_{\mathrm{Ni}}}{m_3\cdot\frac{m_1}{m_2}\cdot\gamma_1\cdot\alpha_{\mathrm{Ni_1}}+m_3\cdot\frac{m_1}{m_2}\cdot\gamma_2\cdot\alpha_{\mathrm{Ni_2}}} \tag{2}$$

$$\beta_{\mathrm{Fe}}=\frac{m_4\cdot\alpha_{\mathrm{Fe}}}{m_3\cdot\frac{m_1}{m_2}\cdot\gamma_1\cdot\alpha_{\mathrm{Fe_1}}+m_3\cdot\frac{m_1}{m_2}\cdot\gamma_2\cdot\alpha_{\mathrm{Fe_2}}} \tag{3}$$

where β_{Ni} and β_{Fe} are recovery rates of Ni and Fe, respectively, %; m_1 is the mass of the unreduced samples, g; m_2 is the mass of the reduced samples, g; m_3 is the mass of the samples before wet ball-milling tests, g; m_4 is the mass of the samples after wet ball-milling tests, g; α_{Fe} and α_{Ni} are the grades of Fe and Ni in magnetic products, respectively, %; $\alpha_{\mathrm{Fe_1}}$ and $\alpha_{\mathrm{Ni_1}}$ are the grades of Fe and Ni in saprolitic laterite ore, respectively, %; $\alpha_{\mathrm{Fe_2}}$ and $\alpha_{\mathrm{Ni_2}}$ are the grades of Fe and Ni in limonitic laterite ore, respectively, %; γ_1 and γ_2 are the mass ratios of saprolitic and limonitic laterite ores in unreduced samples, respectively, %.

3 Results and discussion

3.1 Phase diagram

3.1.1 $CaO-MgO-SiO_2-Al_2O_3$ system

The phase diagram of $CaO-MgO-SiO_2-Al_2O_3$ system is illustrated in Fig. 4 when the mass ratio of $Al_2O_3/(CaO+SiO_2+MgO)$ is maintained at 0.05. The phases in this system mainly include forsterite (Mg_2SiO_4), pyroxene ($MgSiO_3$), diopside ($CaMgSi_2O_6$), wollastonite ($CaSiO_3$), melilite ($Ca_2MgSi_2O_7$) and merwinite ($Ca_3MgSi_2O_8$). When the mass ratio of MgO/SiO_2 is kept at 0.12−0.36 and CaO content is below 15 wt.%, the refractory phases such as

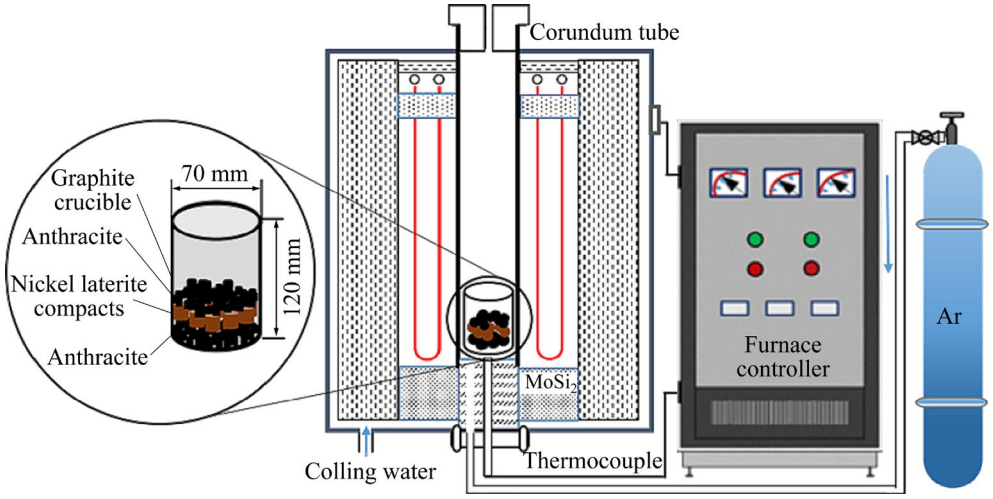

Fig. 3 Schematic diagram of direct reduction test equipment

Mg_2SiO_4 and $MgSiO_3$ are formed. Their melting points are over 1500 °C. The liquidus temperature is reduced to 1300 °C when CaO content is kept at 15−30 wt.%. The predominant phase is in form of $CaMgSi_2O_6$ and its minimum eutectic point temperature is 1278.70 °C. A further increase in CaO content results in the formation of the refractory phases such as $Ca_2MgSi_2O_7$ and $Ca_3MgSi_2O_8$. Thus, CaO content of slag must be appropriate. In this slag system, the phase with the lowest melting temperature is $CaMgSi_2O_6$, which is located in the marked area of *ABCDE* in Fig. 4. The detailed chemical compositions of the marked points are shown in Table 3. However, the MgO/SiO_2 mass ratio in this area is lower than that in the slag system of nickel laterite. The slag compositions are needed to be further optimized.

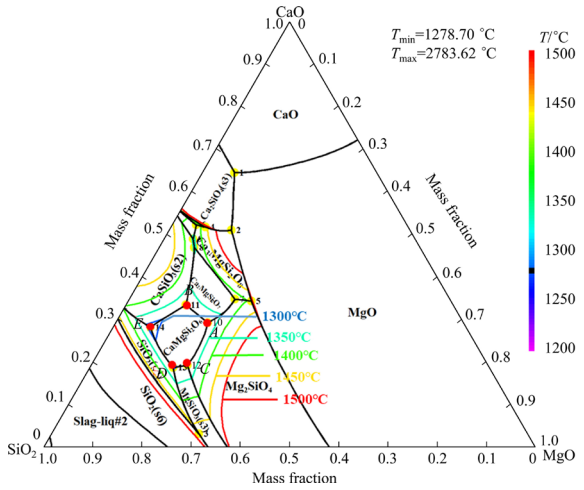

Fig. 4 Phase diagram of CaO−MgO−SiO_2−Al_2O_3 system at Al_2O_3/(CaO+SiO_2+MgO) mass ratio of 0.05

Table 3 Chemical compositions and corresponding temperatures of marked points in Fig. 4

Point	Chemical composition/wt.%				CaO/SiO_2 mass ratio	MgO/SiO_2 mass ratio	Temperature/°C
	CaO	SiO_2	MgO	Al_2O_3			
A	27.80	49.51	17.93	4.76	0.56	0.36	1309.35
B	31.79	51.77	11.68	4.76	0.61	0.23	1308.04
C	18.30	58.25	18.69	4.76	0.31	0.32	1306.41
D	17.76	61.28	16.20	4.76	0.29	0.26	1296.25
E	26.80	61.18	7.26	4.76	0.44	0.12	1278.70

In addition, Al_2O_3 content of slag is increased with the addition of limonitic laterite ore. The phase diagram of CaO−MgO−SiO_2−Al_2O_3 system is presented in Fig. 5 when the mass ratio of CaO/(Al_2O_3+SiO_2+MgO) is set at 0.20. When the MgO/SiO_2 mass ratio is not higher than 0.34 and Al_2O_3 content is below 15 wt.%, the melting temperature of slag is decreased with the increase of Al_2O_3 content. When Al_2O_3 content is kept at 15−20 wt.%, the slag system is located at the liquidus of 1250 °C and the minimum melting temperature is as low as 1202.58 °C. However, the melting temperature of slag is increased with the increase of the Al_2O_3 content when it is over 20 wt.%. The predominant phases are transformed from Mg_2SiO_4 and $MgSiO_3$ to $CaAl_2Si_2O_8$ and $Mg_4Al_{10}Si_2O_{23}$. The melting temperatures of the latter two phases are also increased with the increase of the Al_2O_3 content. In the marked area of *ABCD*, the melting temperature of slag is below 1300 °C. The minimum Al_2O_3 content in this area is 6.09 wt.% as shown in Table 4.

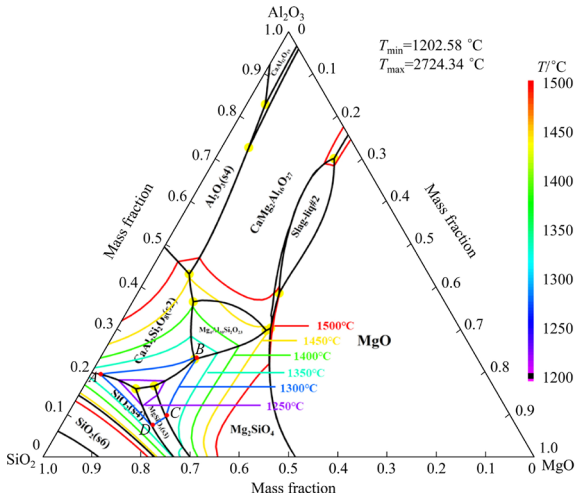

Fig. 5 Phase diagram of CaO−MgO−SiO_2−Al_2O_3 system at CaO/(Al_2O_3+SiO_2+MgO) mass ratio of 0.20

Table 4 Chemical compositions and corresponding temperatures of marked points in Fig. 5

Point	Chemical composition/wt.%				MgO/SiO_2 mass ratio	CaO/SiO_2 mass ratio	Temperature/°C
	CaO	SiO_2	MgO	Al_2O_3			
A	16.67	65.27	1.79	16.27	0.03	0.26	1300.00
B	16.67	47.80	16.02	19.52	0.34	0.35	1300.00
C	16.67	58.42	17.06	7.86	0.29	0.29	1300.00
D	16.67	61.54	15.71	6.09	0.26	0.27	1300.00

3.1.2 CaO−MgO−SiO_2−Al_2O_3−FeO system

As indicated in the previous study [22], the FeO content of slag is increased with the addition of

limonitic laterite ore. The phase diagram of CaO−MgO−SiO_2−Al_2O_3−FeO system is depicted in Fig. 6 when the mass ratios of Al_2O_3/(CaO+SiO_2+MgO) and FeO/(CaO+SiO_2+MgO) are kept at 0.05 and 0.10, respectively. In this marked area, the phase with the minimum melting temperature is still $CaMgSi_2O_6$. However, the minimum eutectic point temperature is reduced from 1278.70 to 1223.44 °C. The melting characteristics of slag can be improved when FeO content is appropriate as shown in Fig. 6 and Table 5. The ideal slag system should consist of 16.00−29.59 wt.% CaO, 46.44−58.07 wt.% SiO_2, 4.43−15.23 wt.% MgO, 4.35 wt.% Al_2O_3 and 8.70 wt.% FeO.

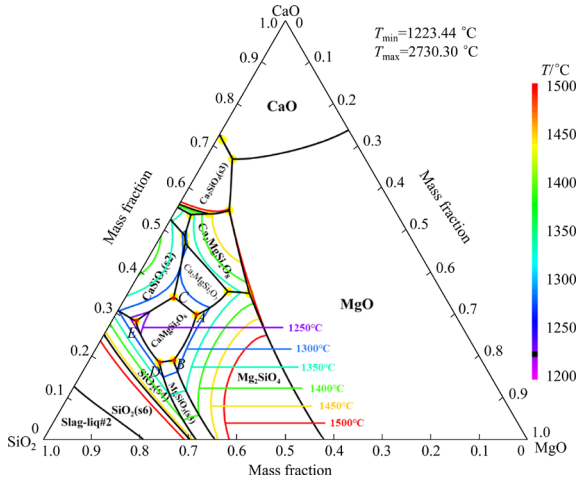

Fig. 6 Phase diagram of CaO−MgO−SiO_2−Al_2O_3−FeO system at Al_2O_3/(CaO+SiO_2+MgO) mass ratio of 0.05 and FeO/(CaO+SiO_2+MgO) mass ratio of 0.10

In addition, high melting-point phases mainly include Mg_2SiO_4 and $MgSiO_3$ in the low-basicity slag. The occurrence of the two phases is adverse to the aggregation and growth of ferronickel grains. When slag basicity is increased to 0.3, $CaMgSi_2O_6$ with the low melting point is easier to be formed. The slag melting characteristics are improved accordingly. When slag basicity is further increased, the high melting-point $Ca_2MgSi_2O_7$ will be formed gradually. Overall, the optimal slag basicity should be 0.3.

3.2 Melting characteristics of slag

The chemical compositions of slag are shown in Table 6. The theoretical melting temperature and liquid phase amount are calculated, as illustrated in Fig. 7. The variations of the actual melting characteristics temperature with slag basicity, limonitic laterite mass fraction and FeO content are shown in Fig. 8.

3.2.1 Effect of slag basicity

Combined with Table 6 and Fig. 7(a_1), the initial melting temperature of slag is obviously increased when slag basicity is increased from 0.01 to 0.30. When slag basicity is further increased, the initial melting temperature of slag is maintained stable. The initial melting temperature of slag is consistently below 1300 °C when slag basicity is kept at 0.10−0.50. In addition, the complete melting temperature of slag is slightly increased when slag basicity is increased from 0.01 to 0.20. When slag basicity is further increased to 0.50, the complete melting temperature of slag is gradually reduced to 1600.74 °C. As shown in Fig. 7(a_2), the liquid phase content of slag reaches over 20 wt.% when slag basicity is 0.10−0.20 and the system temperature is below 1300 °C. $CaMgSi_2O_6$ with the low melting point is mainly formed as indicated in Section 3.1.

As can be seen in Fig. 8(a), the softening temperature of slag is reduced with the increase of slag basicity. The hemisphere temperature and flow temperature of slag are gradually decreased when slag basicity is increased from 0.01 to 0.30. When slag basicity is further increased to 0.50, the two temperatures of slag remain stable. The recommended slag basicity is 0.30.

Table 5 Chemical compositions and corresponding temperatures of marked points in Fig. 6

Point	Chemical composition/wt.%					CaO/SiO_2 mass ratio	MgO/SiO_2 mass ratio	Temperature/°C
	CaO	SiO_2	MgO	Al_2O_3	FeO			
A	25.85	46.44	14.66	4.35	8.70	0.56	0.32	1266.17
B	16.42	55.30	15.23	4.35	8.70	0.30	0.28	1263.60
C	29.59	48.66	8.71	4.35	8.70	0.61	0.18	1260.32
D	16.00	58.07	12.89	4.35	8.70	0.28	0.22	1252.36
E	24.54	57.99	4.43	4.35	8.70	0.42	0.08	1223.44

Table 6 Chemical compositions of slag

Limonitic laterite mass fraction/%	Basicity	Chemical composition/wt.%				
		FeO	MgO	SiO_2	Al_2O_3	CaO
10	0.01	0	40.81	56.11	2.49	0.59
10	0.10	0	38.86	53.43	2.37	5.34
10	0.20	0	36.89	50.72	2.25	10.14
10	0.30	0	35.11	48.27	2.14	14.48
10	0.40	0	33.49	46.05	2.04	18.42
10	0.50	0	32.02	44.02	1.95	22.01
0	0.30	0	35.52	48.47	1.46	14.54
10	0.30	0	35.11	48.27	2.14	14.48
20	0.30	0	34.62	48.03	2.94	14.41
30	0.30	0	34.04	47.75	3.88	14.33
40	0.30	0	33.35	47.42	5.00	14.23
10	0.30	0	35.11	48.27	2.14	14.48
10	0.30	2	34.41	47.30	2.10	14.19
10	0.30	4	33.71	46.34	2.05	13.90
10	0.30	6	33.00	45.37	2.01	13.61
10	0.30	8	32.30	44.41	1.97	13.32

3.2.2 Effect of limonitic laterite mass fraction

The effect of limonitic laterite mass fraction on the melting characteristics of slag is revealed at the slag basicity of 0.30, as shown in Figs. 7(b_1), 7(b_2) and 8(b). When limonitic laterite mass fraction is increased from 0 to 40%, the initial melting temperature and complete melting temperature of slag are reduced from 1298.57 and 1645.17 °C to 1258.18 and 1608.76 °C, respectively. In addition, Al_2O_3 content of slag is increased from 1.46 wt.% to 5.00 wt.%. As confirmed in Fig. 5, the melting temperature of slag is reduced with the increase of the Al_2O_3 content when it is below 15 wt.%. The liquid phase content of slag is gradually increased with limonitic laterite mass fraction at the same temperature as shown in Fig. 7(b_2). Combined with the illustration in Fig. 8(b), the softening temperature, hemisphere temperature and flow temperature of slag are all reduced with the increase of the limonitic laterite mass fraction. Overall, the melting characteristics of slag are more appropriate when limonitic laterite mass fraction is not less than 10%.

3.2.3 Effect of FeO content of slag

When slag basicity is 0.30 and limonitic laterite mass fraction is 10%, the variations of slag melting characteristics with FeO content are illustrated in Figs. 7(c_1), (c_2) and 8(c). As shown in Fig. 7(c_1), the initial melting temperature of slag is obviously reduced with the increase of FeO content. However, the complete melting temperature of slag remains stable overall. When the temperature is below 1325 °C, as shown in Fig. 7(c_2), liquid phase is easier to be formed with the increase of FeO content. In addition, the softening temperature, hemisphere temperature and flow temperature of slag are all reduced when FeO content is increased from 0 to 8 wt.%, as shown in Fig. 8(c). Overall, slag melting characteristics are improved with the increase of FeO content.

3.3 Optimized parameters of semi-molten smelting process

3.3.1 Grades and recoveries of Ni and Fe

The effect of reduction temperature on the grades and recovery rates of Ni and Fe is depicted in Fig. 9(a) when C/O mass ratio, slag basicity and limonitic laterite mass fraction are 0.86, 0.3 and 20%, respectively. When the reduction temperature is increased from 1250 to 1325 °C, Fe grade is increased from 81.55% to 89.36%. The recovery rates of Ni and Fe are increased from 65.33% and 69.21% to 88.91% and 75.36%, respectively. In addition, Ni grade is increased from 4.26% to 6.42% when the reduction temperature is increased from 1250 to 1275 °C. However, Ni grade is slightly decreased to 6.21% with the further increase of reduction temperature to 1325 °C. Overall, the appropriate reduction temperature is 1300 °C.

Figure 9(b) illustrates the effect of C/O mass ratio on the grades and recovery rates of Ni and Fe when the reduction temperature, slag basicity and limonitic laterite mass fraction are 1300 °C, 0.3 and 20%, respectively. When C/O mass ratio is increased from 0.8 to 1.1, the recovery rates of Ni and Fe are gradually decreased from 88.85% and 72.44% to 84.68% and 70.53%, respectively. Meanwhile, Fe grade is increased from 82.32% to 87.56% and Ni grade remains stable. Overall, the appropriate C/O mass ratio is 0.86. The recovery rates of Ni and Fe reach 88.60% and 72.25%, respectively. The grades of Ni and Fe are 6.42% and 86.99%, respectively.

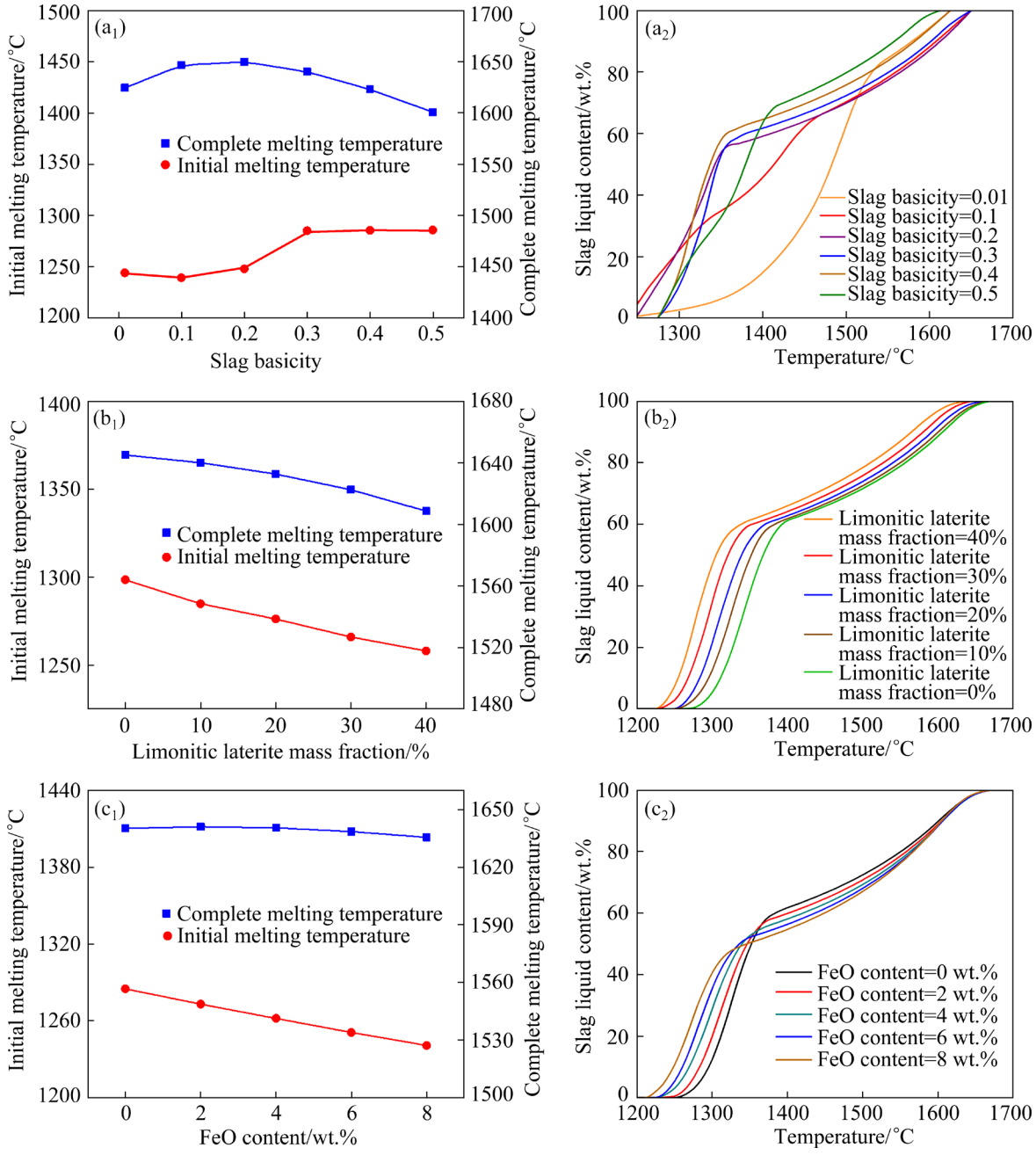

Fig. 7 Effect of slag basicity (a_1, a_2), limonitic laterite mass fraction (b_1, b_2) and FeO content (c_1, c_2) of slag on theoretical melting temperature (a_1–c_1) and slag liquid content (a_2–c_2)

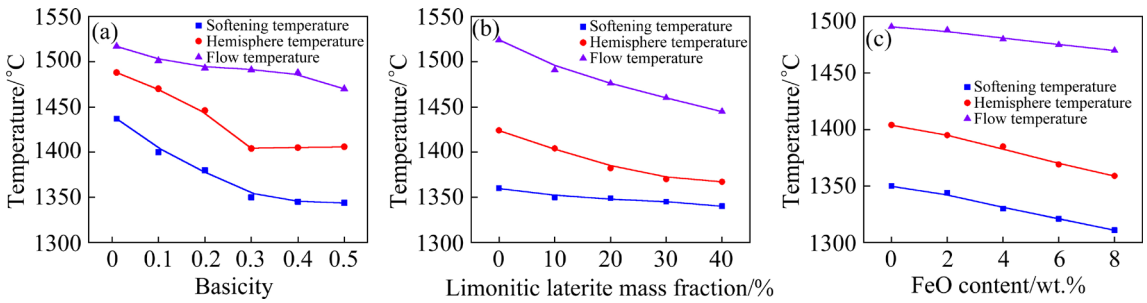

Fig. 8 Effect of slag basicity (a), limonitic laterite mass fraction (b) and FeO content (c) of slag on actual characteristic temperature during smelting process

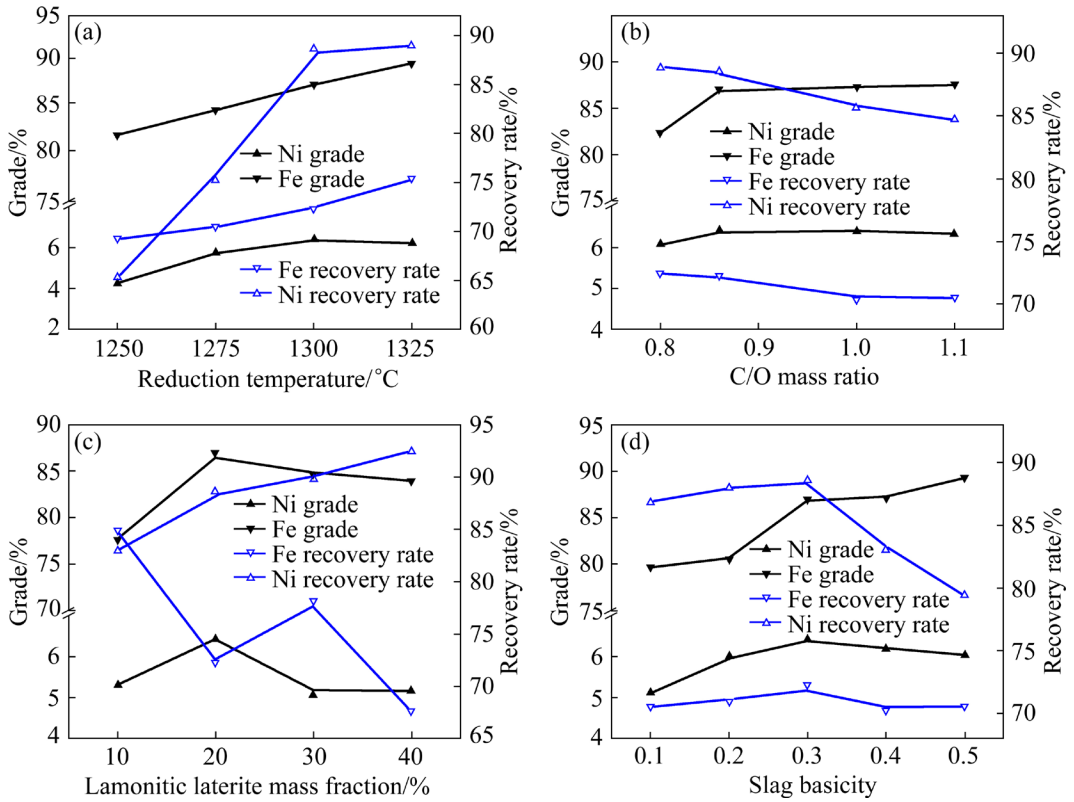

Fig. 9 Effect of reduction temperature (a), C/O mass ratio (b), limonitic laterite mass fraction (c) and slag basicity (d) on grades and recovery rates of Ni and Fe

As shown in Fig. 9(c), the limonitic laterite mass fraction is optimized when the reduction temperature, C/O mass ratio and slag basicity are kept at 1300 °C, 0.86 and 0.3, respectively. The recovery rate of Ni is increased with the increase of the limonitic laterite mass fraction. However, the recovery rate of Fe is overall reduced. When limonitic laterite mass fraction is increased from 10% to 20%, the grades of Ni and Fe are increased from 5.31% and 77.62% to 6.42% and 86.99%, respectively. When limonitic laterite mass fraction is further increased, the two grades are both decreased. The recommended limonitic laterite mass fraction is 20%.

As shown in Fig. 9(d), the effect of slag basicity is investigated when the reduction temperature, C/O mass ratio and limonitic laterite mass fraction are 1300 °C, 0.86 and 20%, respectively. When slag basicity is increased from 0.1 to 0.3, Ni grade is increased from 5.11% to 6.05%. The recovery rates of Ni and Fe are increased from 86.85% and 70.52% to 88.60% and 72.25%, respectively. When slag basicity is further increased to 0.5, the three indices are decreased to 6.05%, 79.41% and 70.56%, respectively. Additionally, Fe grade is increased with the increase of the slag basicity. Overall, the optimum values of reduction temperature, C/O mass ratio, limonitic laterite mass fraction and slag basicity are 1300 °C, 0.86, 20% and 0.3, respectively. The recovery rates of Ni and Fe reach 88.60% and 72.25%, respectively. The grades of Ni and Fe in ferronickel products are 6.42% and 86.99%, respectively.

3.3.2 Growth characteristics of ferronickel grains

As illustrated in Fig. 10(a), the deformation degree of reduced briquettes is gradually increased with the increase of limonitic laterite mass fraction. At the limonitic laterite mass fraction of 20%, a distinct deformation can be observed. When the limonitic laterite mass fraction is further increased, the shape of reduced briquettes is increasingly irregular and the volume of reduced briquettes is further decreased. This is mainly due to the crystalline water decomposition and excessive liquid phase formation. Similarly, a significant deformation can be observed in reduced briquettes

when slag basicity exceeds 0.3, as shown in Fig. 10(b).

Figures 11 and 12 show that the average diameter of ferronickel grains in reduced briquettes is increased with the increase of the limonitic laterite mass fraction and slag basicity. In addition, the increased extent of the average diameter of ferronickel grains is notably greater when limonitic laterite mass fraction and slag basicity are not higher than 20% and 0.3, respectively. This is mainly due to the increase of liquid phase amount and the improvement of melting characteristics of slag. Ferronickel products are easier to be obtained when limonitic laterite mass fraction and slag basicity are maintained at 20% and 0.3, respectively.

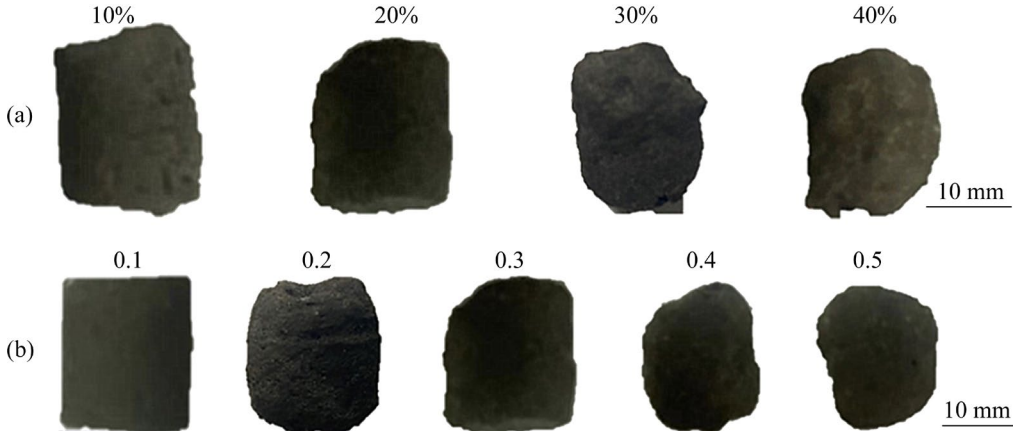

Fig. 10 Macro-images of reduced briquettes: (a) Effect of limonitic laterite mass fraction; (b) Effect of slag basicity

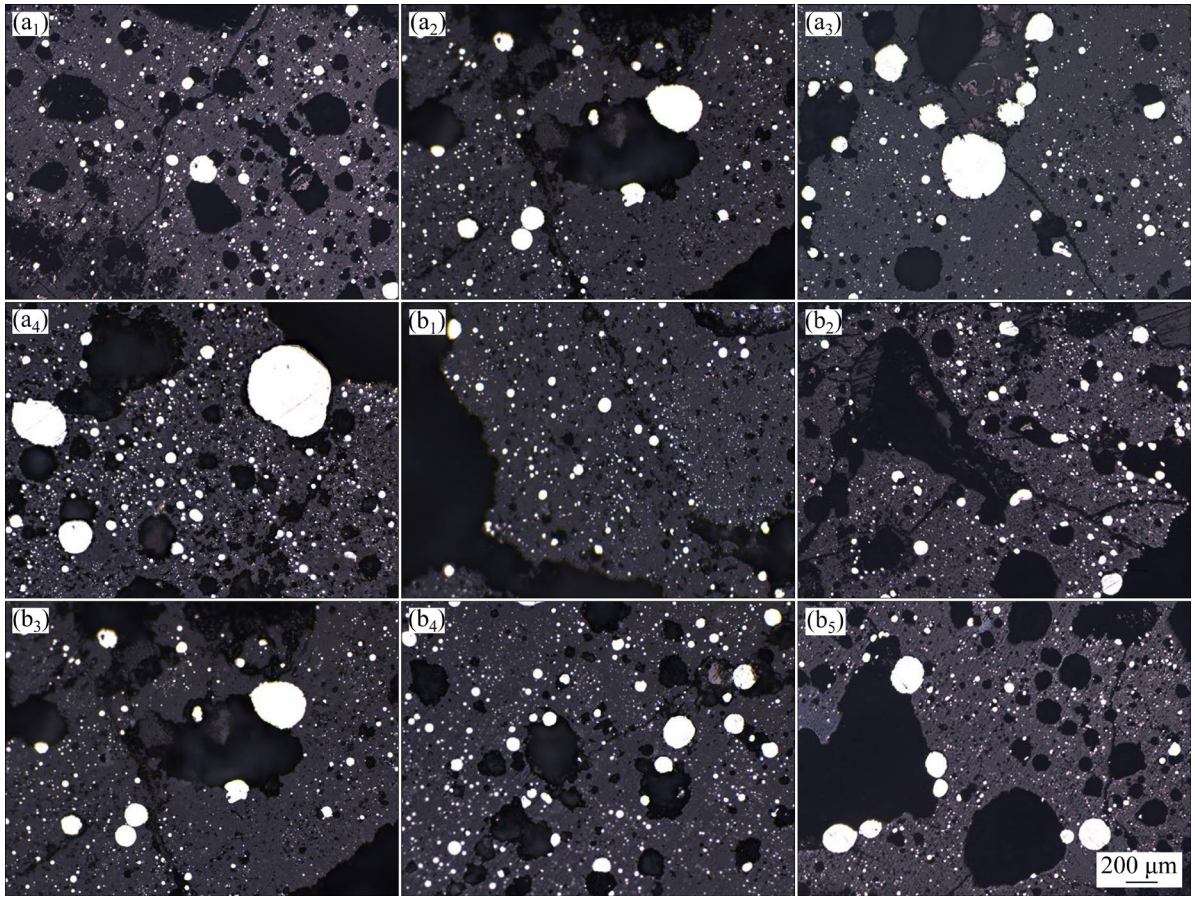

Fig. 11 Microstructures of reduced briquettes: (a_1−a_4) Limonitic laterite mass fractions of 10%, 20%, 30% and 40%, respectively; (b_1−b_5) Slag basicities of 0.1, 0.2, 0.3, 0.4 and 0.5, respectively

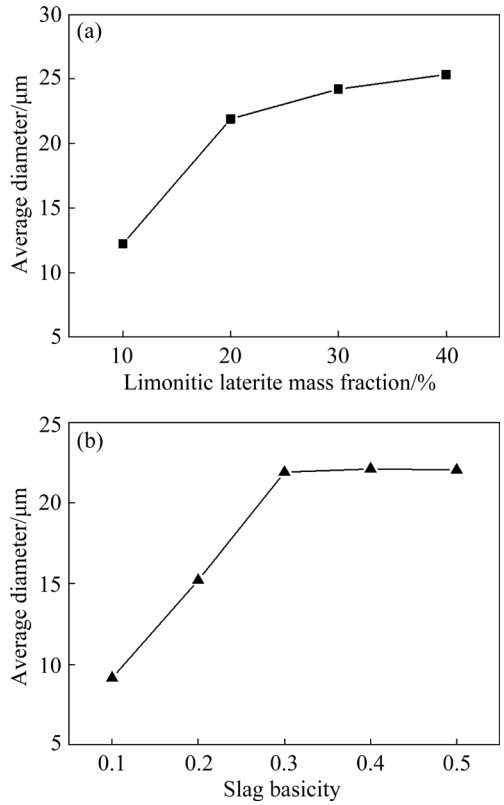

Fig. 12 Average diameter of ferronickel grains in reduced briquettes: (a) Effect of limonitic laterite mass fraction; (b) Effect of slag basicity

4 Conclusions

(1) The phase diagram analysis indicates that the minimum eutectic point temperature of slag system can be decreased to 1223.44 °C by adjusting the contents of CaO, Al_2O_3, and FeO. In the low melting-point region of $CaMgSi_2O_6$, the mass ratios of CaO/SiO_2 and MgO/SiO_2 are kept at 0.28−0.61 and 0.08−0.32 when the contents of FeO and Al_2O_3 are 8.70 wt.% and 4.35 wt.%, respectively.

(2) The melting characteristics of slag can be significantly improved when slag basicity is maintained at 0.3 and limonitic laterite mass fraction is not less than 10%. The melting characteristics of slag are also improved with the increase of FeO content.

(3) The aggregation and growth of ferronickel grains are more adequate when the reduction temperature, C/O mass ratio, limonitic laterite mass fraction and slag basicity are kept at the optimum values of 1300 °C, 0.86, 20% and 0.3, respectively. The grades of Ni and Fe in ferronickel products reach 6.42% and 86.99%, respectively, and the recovery rates of Ni and Fe are 88.60% and 72.25%, respectively.

CRediT authorship contribution statement

Yu-xiao XUE: Writing − Original draft, Review & editing, Funding acquisition; **Jian-bo ZHAO:** Investigation, Data curation; **Zhi-xiong YOU:** Writing − Review & editing, Methodology, Funding acquisition; **Xue-wei LV:** Methodology, Conceptualization.

Declaration of competing interest

The authors declare that they have no known competing financial interests or personal relationships that could have appeared to influence the work reported in this paper.

Acknowledgments

Financial supports from the National Key R&D Program of China (No. 2022YFC3901404), the Natural Science Foundation of Chongqing, China (No. CSTB2023NSCQ-BHX0166), and the Fundamental Research Funds for the Central Universities, China (No. 2023CDJXY-016) are sincerely acknowledged.

References

[1] RAO Ming-jun, LI Guang-hui, JIANG Tao, LUO Jun, ZHANG Yuan-bo, FAN Xiao-hui. Carbothermic reduction of nickeliferous laterite ores for nickel pig iron production in China: A review [J]. JOM, 2013, 65(11): 1573−1583.

[2] KLYUSHNIKOV A, SERGEEVA S, GULYAEVA R, VUSIKHIS A, UDOEVA L, TYUSHNYAKOV S. Viscosity of slags from joint smelting of oxidized nickel and sulfide copper ores [J]. Transactions of Nonferrous Metals Society of China, 2023, 33(10): 3168−3184.

[3] LIU Peng-jun, LIU Zheng-gen, CHU Man-sheng, YAN Rui-jun, LI Feng, TANG Jue. Multiobjective collaborative optimization of novel carbothermal reduction process of stainless steel dust and laterite nickel ore [J]. Transactions of Nonferrous Metals Society of China, 2023, 33(6): 1919−1931.

[4] XUE Yu-xiao, ZHU De-qing, PAN Jian, LI Gen, LV Xue-wei. Reduction of carbon footprint through hybrid sintering of low-grade limonitic nickel laterite and chromite ore [J]. Journal of Sustainable Metallurgy, 2023, 9(2): 648−664.

[5] CHENG Gong-jin, TANG Wei-dong, XUE Xiang-xin. Effect of nickel oxide additive on smelting mechanism of chromium-bearing vanadium titanomagnetite pellets [J]. Transactions of Nonferrous Metals Society of China, 2021, 31(8): 2501−2510.

[6] WEI Wen-jing, SAMUELSSON P B, TILLIANDER A, GYLLENRAM R, JÖNSSON P G. Energy consumption and greenhouse gas emissions of nickel products [J]. Energies, 2020, 13(21): 5664.

[7] WARNER A E M, DÍAZ C M, DALVI A D, MACKEY P J, TARASOV A V. JOM world nonferrous smelter survey. Part III: Nickel: Laterite [J]. JOM, 2006, 58(4): 11−20.

[8] YANG Wei-jiao, MA Bao-zhong, LI Xiang, HU Die, WANG

Cheng-yan, WANG Hua. Transferring behavior and reaction kinetics of saprolitic laterite during metalized reduction in the presence of calcium fluoride [J]. Minerals Engineering, 2022, 176: 107353.
[9] LI Bo, WANG Hua, WEI Yong-gang. The reduction of nickel from low-grade nickel laterite ore using a solid-state deoxidisation method [J]. Minerals Engineering, 2011, 24(14): 1556−1562.
[10] MA Dong-lai, ZHAO Jian-bo, HU Qing-qing, LÜ Xue-ming, YOU Yang, YOU Zhi-xiong, LÜ Xue-wei. Effect of additives on growth of ferronickel grains and metal−slag separation behavior [J]. Transactions of Nonferrous Metals Society of China, 2022, 32(10): 3459−3468.
[11] ZHANG Qiang, SUN Yong-sheng, HAN Yue-xin, LI Yan-jun, GAO Peng. Review on coal-based reduction and magnetic separation for refractory iron-bearing resources [J]. International Journal of Minerals, Metallurgy and Materials, 2022, 29(12): 2087−2105.
[12] LV Xue-ming, LV Wei, LIU Mei, YOU Zhi-xiong, LV Xue-wei, BAI Cheng-guang. Effect of sodium sulfate on preparation of ferronickel from nickel laterite by carbothermal reduction [J]. ISIJ International, 2018, 58(5): 799−807.
[13] GAO Li-hua, LIU Zheng-gen, PAN Yu-zhu, GE Yang, FENG Cong, CHU Man-sheng, TANG Jue. Separation and recovery of iron and nickel from low-grade laterite nickel ore using reduction roasting at rotary kiln followed by magnetic separation technique [J]. Mining, Metallurgy & Exploration, 2019, 36(2): 375−384.
[14] ABDUL F, DEVALINI P M, SETIYORINI Y, SETYOWATI V A, PINTOWANTORO S. Effect of inner reductant addition and laying on carbothermic reduction process of laterite nickel ore/coal composite briquette [J]. Arabian Journal for Science and Engineering, 2023, 48(9): 11285−11294.
[15] QUINTERO-CORONEL D A, GUILLIN-ESTRADA W D, ECHEVERRI-ROMAN J L, MAURY H, CORREDOR L, RUIZ J A, RUEDA B S, GONZALEZ-QUIROGA A. Large- and particle-scale energy assessment of reduction roasting of nickel laterite ore for ferronickel production via the rotary kiln-electric furnace process [J]. Thermal Science and Engineering Progress, 2022, 32: 101331.
[16] MA Bao-zhong, LI Xiang, YANG Wei-jiao, HU Die, XING Peng, LIU Bao, WANG Cheng-yan. Nonmolten state metalized reduction of saprolitic laterite ores: Effective extraction and process optimization of nickel and iron [J]. Journal of Cleaner Production, 2020, 256: 120415.
[17] WANG Lun-wei, LÜ Xue-ming, LIU Mei, YOU Zhi-xiong, LÜ Xue-wei, BAI Chen-guang. Preparation of ferronickel from nickel laterite via coal-based reduction followed by magnetic separation [J]. International Journal of Minerals, Metallurgy, and Materials, 2018, 25(7): 744−751.
[18] NURJAMAN F, AMELY I, ASTUTI W, SUHARNO B. The effect of ternary basicity ($CaO/(Al_2O_3+SiO_2)$) on selective reduction of limonitic nickel ore [J]. Advances in Materials and Processing Technologies, 2022, 8(Suppl.): 763−773.
[19] JU P, RYOM K, HONG K. Separation of iron-nickel alloy nugget from limonitic laterite ore using self-reduction [J]. Journal of Mining and Metallurgy (Section B): Metallurgy, 2018, 54(3): 385−392.
[20] ZHANG Ying-yi, CUI Kun-kun, WANG Jie, WANG Xun-fu, QIE Jun-mao, XU Qi-yan, QI Yuan-hong. Effects of direct reduction process on the microstructure and reduction characteristics of carbon-bearing nickel laterite ore pellets [J]. Powder Technology, 2020, 376: 496−506.
[21] SUHARNO B, NURJAMAN F, OEDIYANI S, HANDOKO A S, BAHFIE F, QAULANHAQ A F, ASTUTI W, PRASETYO E. Kinetic study in selective reduction of limonitic and saprolitic nickel ore [J]. Canadian Metallurgical Quarterly, 2023, 62(3): 602−616.
[22] LV Xue-ming, WANG Lun-wei, YOU Zhi-xiong, YU Wen-zhou, LV Xue-wei. A novel method of smelting a mixture of two types of laterite ore to prepare ferronickel [J]. JOM, 2019, 71(11): 4191−4197.
[23] TIAN Hong-yu, PAN Jian, ZHU De-qing, YANG Cong-cong, GUO Zheng-qi, XUE Yu-xiao. Improved beneficiation of nickel and iron from a low-grade saprolite laterite by addition of limonitic laterite ore and $CaCO_3$ [J]. Journal of Materials Research and Technology, 2020, 9(2): 2578−2589.
[24] RAO Ming-jun, LI Guang-hui, ZHANG Xin, LUO Jun, PENG Zhi-wei, JIANG Tao. Reductive roasting of nickel laterite ore with sodium sulfate for Fe−Ni production. Part I: Reduction/sulfidation characteristics [J]. Separation Science and Technology, 2016, 51(8): 1408−1420.

炉渣碱度对腐殖土型与褐铁矿型红土镍矿半熔融法冶炼的影响

薛钰霄[1,2]，赵剑波[1,2]，游志雄[1,2]，吕学伟[1,2]

1. 重庆大学 材料科学与工程学院，重庆 400044；
2. 重庆大学 钒钛冶金及新材料重庆市重点实验室，重庆 400044

摘　要：系统分析了炉渣碱度对腐殖土型与褐铁矿型红土镍矿半熔融法冶炼的影响。当炉渣碱度为 0.3、褐铁矿型红土镍矿质量分数不低于10%的条件下，炉渣成分可位于低熔点透辉石($CaMgSi_2O_6$)的液相线区。在最佳冶炼参数条件下，即还原温度为 1300 ℃、C/O 质量比为 0.86、褐铁矿型红土镍矿质量分数为 20%及炉渣碱度为 0.3，制备了镍品位为 6.42%、铁品位为 86.99%的镍铁产品，且镍与铁的回收率分别达到 88.60%和 72.25%。

关键词：镍铁；腐殖土型红土镍矿；褐铁矿型红土镍矿；炉渣碱度；半熔融工艺

(Edited by Wei-ping CHEN)